ChemComm

COMMUNICATION

View Article Online
View Journal | View Issue

Cite this: *Chem. Commun.*, 2022, **58**, 7176

Received 14th March 2022,
Accepted 27th May 2022

DOI: 10.1039/d2cc01470j

rsc.li/chemcomm

Reduction of N_2O with hydrosilanes catalysed by RuSNS nanoparticles†

Pablo Molinillo,[a] Bertrand Lacroix,[bc] Florencia Vattier,[d] Nuria Rendón,*[a] Andrés Suárez*[a] and Patricia Lara*[a]

A series of RuSNS nanoparticles, prepared by decomposition of Ru(COD)(COT) with H_2 in the presence of an SNS ligand, have been found to catalyse the reduction of the greenhouse gas N_2O to N_2 employing different hydrosilanes.

Nitrous oxide (N_2O) is a potent ozone-depleting, greenhouse gas, with a climate warming impact three hundred times that of carbon dioxide.[1,2] The increasing concentration of this gas in the Earth's atmosphere is attributed to human activities involving the use of fertilizers, the large-scale combustion of fossil fuels and biomass, and industrial chemical processes that produce it as a by-product.[3] Therefore, there is a significant interest in the development of chemical transformations for the degradation of N_2O into non-harmful species,[4] as well as for its revalorization as a chemical feedstock in the context of a circular economy.[5] A procedure for N_2O mitigation consists of the hydrogenation of this molecule to innocuous nitrogen gas (N_2) and water, which can be carried out using heterogeneous catalysts operating under relatively harsh conditions.[6] Moreover, transition metal complexes have also been recently demonstrated to catalyse the hydrogenation[7,8] and the hydroboration[9] of N_2O.

Although lacking the future prospects of clean, large-scale production of H_2 from renewable sources, hydrosilanes are commonly employed as reducing agents in both academic laboratories and industrial settings since reduction of a large diversity of compounds, including small gas molecules such as CO_2,[10] can be efficiently performed.[11] Advantages associated with the use of silanes as reducing agents include their low cost, easy handling and for some derivatives, as in the case of poly(methylhydrosiloxane) (PMHS), their attributed low environmental impact. However, the reduction of N_2O with silanes has only been briefly investigated. In 2017, Milstein *et al.* made use of a Ru-PNP pincer complex in the reduction of N_2O with $PhMe_2SiH$, Ph_2MeSiH and $^tBuMe_2SiH$.[7] Reactions were carried out using 1–2 mol% Ru at 65 °C under 3.4 bar of N_2O for 36–72 h. Recently, Cantat *et al.* reported a metal-free reduction of N_2O using disilanes.[12] It is also worth noting that oxidation of hydrosilanes with N_2O leads to the formation of technologically important Si–O containing derivatives, such as silanols and siloxanes, with applications in the synthesis of silicon-based polymeric materials as well as reagents in organic synthesis.[13] This process could contribute to the use of waste N_2O in the context of a circular economy, and complement current methods for silane oxidation based on the use of H_2O, H_2O_2 and O_2.[14]

Metal nanoparticles (NPs) have been widely employed in a diverse range of catalytic processes due to their particular electronic configurations and much larger surface areas when compared with bulk metals.[15] The preparation of NPs through the decomposition of an organometallic precursor with H_2 in the presence of substoichiometric amounts of a ligand, as pioneered by Chaudret, Philippot *et al.*, provides materials possessing well-controlled size, shape and surface state.[16] Herein, we report on the synthesis and characterization of a series of Ru NPs stabilized with readily available SNS ligands. More interestingly, based on the known reactivity of related NPs in hydrosilylation reactions,[17] these nanocatalysts have been tested in the reduction of N_2O with hydrosilanes.

Ru·**L** NPs were easily synthesized by exposing THF solutions of Ru(COD)(COT), (1,5-cyclooctadiene)(1,3,5-cyclooctatriene)-ruthenium(0), to 3 bar of H_2 in the presence of the SNS ligands **L1–L4**[18] (Scheme 1). Different ligand/metal ratios were explored to obtain well-controlled metal nanoparticles. Thus, a series of colloids were prepared using 0.5 equiv of **L1–L4**. In all the cases, small and well-dispersed crystalline nanoparticles

[a] *Instituto de Investigaciones Químicas (IIQ), Departamento de Química Inorgánica, and Centro de Innovación en Química Avanzada (ORFEO-CINQA), CSIC and Universidad de Sevilla. Avda. Américo Vespucio 49, 41092 Sevilla, Spain. E-mail: patricia@iiq.csic.es*
[b] *Department of Material Science and Metallurgic Engineering, and Inorganic Chemistry, University of Cádiz, Spain*
[c] *IMEYMAT: Institute of Research on Electron Microscopy and Materials of the University of Cádiz, Spain*
[d] *Instituto de Ciencia de Materiales de Sevilla, CSIC-Universidad de Sevilla. Avda. Américo Vespucio 49, 41092 Sevilla, Spain*

† Electronic supplementary information (ESI) available: Synthesis and characterization of Ru NPs. Catalytic procedures. NMR data of catalytic reaction products. See DOI: https://doi.org/10.1039/d2cc01470j

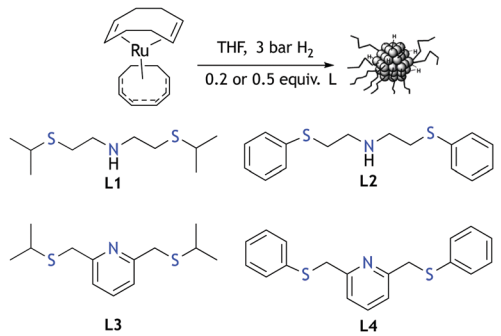

Scheme 1 Preparation of Ru·**L** NPs, and SNS ligands employed as stabilizers.

exhibiting mean sizes between 1.5 and 1.9 nm were obtained, as revealed by TEM (Fig. 1 and Fig. S1–S6, ESI†). The metal content (32–47% Ru) in the nanoparticles was determined by inductive coupled plasma (ICP) analysis of the purified materials. Attempts to obtain monodispersed nanoparticles using lower amounts of ligand, *i.e.* 0.2 equiv, yielded agglomerated metal, with the exception of **L4** that led to the main formation of small and monodispersed nanoparticles (mean size: 2.3 (0.4) nm) along with slight metal agglomeration, as observed on the TEM grid (Fig. S7 and S8, ESI†). As observed previously for Ru NPs, the mean size of the particles slightly decreases upon using higher ligand/metal ratios.[19]

The crystalline character of the Ru·**L** NPs thus prepared is clearly demonstrated by HRTEM observations for Ru·**L2**$^{0.5}$ (Fig. S11, ESI†) and Ru·**L4**$^{0.5}$ (Fig. 2). The fast Fourier transform (FFT) analysis of the micrographs shows interplanar spacings and angles that correspond to a ruthenium hexagonal close-packed (hcp) structure. In addition, the observation of some NPs along the [10−10] and [0001] zone axis clearly reveals the presence of (0001), {01−11} and {01−10} crystal facets.

For samples Ru·**L2**$^{0.5}$ and Ru·**L4**$^{0.5}$, the Ru composition of the NPs was confirmed by the EDX spectra and elemental map (Fig. S12 and Fig. 3, respectively). EDX also reveals (more particularly for the Ru·**L2**$^{0.5}$ sample) the presence of S expected to come from the SNS ligands, and O that could indicate oxidation of the NP surface. Although mostly detected in the NP regions, S and O signals are also spotted in between the NPs which could be explained by decomposition under the electron beam.

The nature and composition of the Ru·**L** nanoparticle surfaces were analysed using XPS (see ESI†). As is well known, the

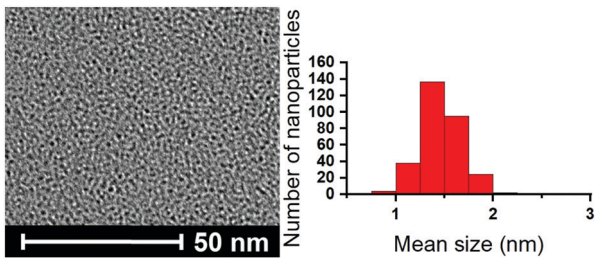

Fig. 1 TEM image with the corresponding size distribution histogram for Ru·**L1**$^{0.5}$.

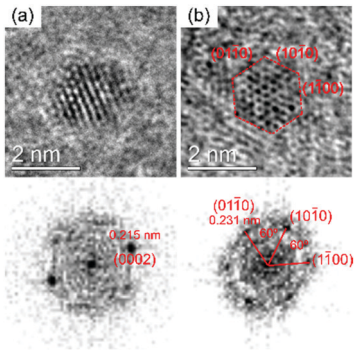

Fig. 2 Top: HRTEM images of single Ru·**L4**$^{0.5}$. Bottom: Fast Fourier transforms with the extracted interplanar distances and angles characteristic of the Ru hcp structure. In (b), the Ru NPs are viewed along the [10−10] and [0001] zone axis, respectively.

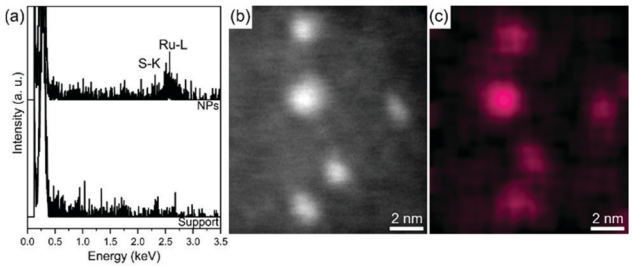

Fig. 3 STEM-EDX results for the Ru·**L4**$^{0.5}$ NPs: (a) EDX spectra recorded over various NPs and over the support (for reference). (b) STEM-HAADF image. (c) Ru·**L4**$^{0.5}$ intensity map using the Ru–L line.

main photoemission peak for ruthenium atoms is the Ru3d signal, although this peak is very close and partially overlaps with the C1s peak. For this reason, the Ru3p photoemission signal is preferred for analysis.[20] Fig. 4 shows the high-resolution spectra for the Ru3p, N1s, and S2p regions for the Ru·**L1**$^{0.5}$ and Ru·**L2**$^{0.5}$ nanoparticles. For the Ru·**L1**$^{0.5}$ and Ru·**L2**$^{0.5}$ samples, high-resolution N1s peaks were found around 400 eV in binding energy (BE) and the S2p photoemission

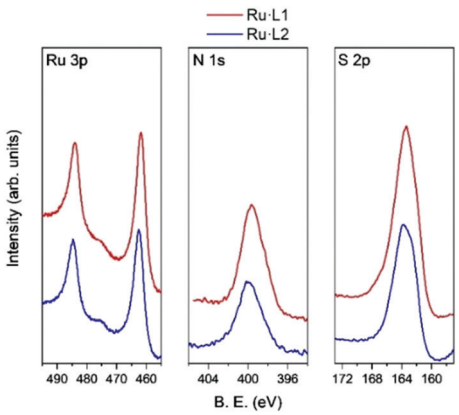

Fig. 4 High-resolution spectra for Ru3p, N1s and S2p of Ru·**L1**$^{0.5}$ and Ru·**L2**$^{0.5}$.

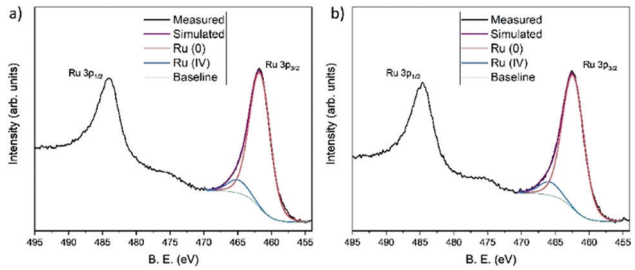

Fig. 5 Experimental and fitted XPS spectra of the Ru3p$_{3/2}$ regions for samples Ru·**L1**$^{0.5}$ (a) and Ru·**L2**$^{0.5}$ (b).

signal shows a wide peak centered at 163.5 eV. The Ru3p signal of Ru·**L1**$^{0.5}$ exhibits two peaks centered at 462.1 and 484.2 eV BE corresponding to 3p$_{3/2}$ and 3p$_{1/2}$ photoemission peaks, respectively. Ru·**L2**$^{0.5}$ shows these peaks at 462.5 and 484.6 eV BE. As shown in Fig. 5a, the high-resolution Ru 3p$_{3/2}$ region for Ru·**L1**$^{0.5}$ is well-fitted with two components at 461.9 and 465.1 eV, corresponding to the Ru(0) and Ru(IV) oxidation states, respectively.[20,21] Likewise, the Ru·**L2**$^{0.5}$ species shows the Ru(0) 3p$_{3/2}$ signal at 462.3 eV, and at 465.7 eV for Ru(IV) (Fig. 5b). The surface oxidation ratio of the nanoparticles Ru·**L1**$^{0.5}$ and Ru·**L2**$^{0.5}$ was found to be very similar, *i.e.* 9% of Ru(IV). Finally, the separation between the major peaks due to spin–orbit splitting took a value of 22.3 eV, in both analyzed species. These results are in agreement with those previously observed in similar size Ru(0) nanoparticles.[22]

The quantification of Ru, N, and S atoms on the surface of the nanoparticles was estimated by means of the relative intensities of the corresponding photoemission signals (Table 1). The N/S ratio is similar and very close to that expected for the stoichiometry of both ligands. This fact enables us to rule out adverse effects during the XPS analysis, such as fragmentation or decomposition of organic compounds. The value of the Ru/N ratio can be correlated to the degree of coverage of the nanoparticle surface by the N-coordinating ligands. Moreover, it could depend on the size of the Ru nanoparticles, although in these cases we have found very similar sizes as determined by TEM. Ru·**L2**$^{0.5}$ is less covered than Ru·**L1**$^{0.5}$, *i.e.* a higher Ru/N ratio, and this could explain its higher observed catalytic activity since it leaves more metal exposed to the reactants (*vide infra*).

The SNS-stabilized Ru nanoparticles were tested in the reduction of N_2O with silanes. Initial experiments were performed using 1.0 mol% of Ru at 55 °C under 1 bar of N_2O, employing $PhMe_2SiH$ (**1a**) (Table 2). While the nanoparticles synthetic precursor Ru(COD)(COT) provided a low silane conversion (entry 1), the reaction with Ru·**L1**$^{0.5}$ took place with 76% conversion (based on silane), leading to a mixture of the corresponding silanol (**2a**) and siloxane (**3a**) in a 4 : 6 ratio,

Table 1 Quantitative analysis of the surface composition of nanoparticles Ru·**L1**$^{0.5}$ and Ru·**L2**$^{0.5}$ (percentage in atomic concentration, % At)

Ru·**L**	Ru (% At)	N (% At)	S (% At)	N/S ratio	Ru/N ratio
Ru·**L1**$^{0.5}$	31.6	21.8	45.3	0.48	1.5
Ru·**L2**$^{0.5}$	37.8	19.7	42.5	0.46	1.9

Table 2 Reduction of N_2O with $PhMe_2SiH$ using Ru·**L** nanoparticles

Entry	Ru cat.	SiH conv. [%]	**2a** : **3a** ratio
1	Ru(COD)(COT)	<5	—
2	Ru·**L1**$^{0.5}$	76	40 : 60
3	Ru·**L2**$^{0.5}$	>99	12 : 88
4	Ru·**L3**$^{0.5}$	>99	25 : 75
5	Ru·**L4**$^{0.5}$	>99	20 : 80
6	Ru·**L4**$^{0.2}$	28	50 : 50

Reaction conditions: 1.0 mol% Ru, 1 bar N_2O, 55 °C, THF. Reaction time: 24 h. Conversion and selectivity were determined by ^{1}H NMR spectroscopy using mesitylene as the internal standard. N_2 formation was detected by GC-MS analysis of the headspace gas (see ESI).

respectively (entry 2). Testing of other catalysts prepared using Ru/L ratios of 0.5 led to complete silane conversions with silanol:siloxane ratios ranging between 12 : 88 and 25 : 75 (entries 3–5); meanwhile, the Ru·**L4**$^{0.2}$ nanoparticles showed a decreased conversion (entry 6). TEM analysis of the reaction with Ru·**L4**$^{0.5}$ reveals that the size of the Ru NPs remains practically constant after the catalytic reactions (mean size 1.5 (0.3) nm; Fig. S9 and S10, ESI†).

Next, other hydrosilanes were tested as reductants using Ru·**L4**$^{0.5}$ as a representative catalyst (Table 3). Complete silane conversion and a high selectivity towards the formation of the silanol **2b** were observed in the reaction with Ph_2MeSiH (**1b**) (entry 1). In marked contrast, the use of dimethylphenethylsilane (**1c**) led to the opposite product distribution, with the siloxane **3c** formed with >99% selectivity. In addition, the reaction of N_2O with tripropylsilane (**1d**) proceeded with a conversion of 95% with the formation of **2d** and **3d** in a 6 : 4 ratio, respectively; whereas no conversion was observed upon using bulky $^iPr_3SiH$ (**1e**). Finally, the reaction with triethoxysilane (**1f**) took place with a high conversion leading to the corresponding silanol and siloxane derivatives in a 6 : 4 ratio (entry 5).

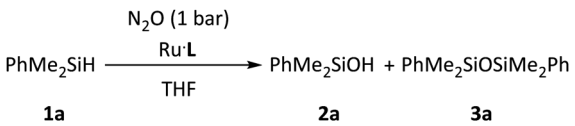

To get insight into the formation of the siloxane derivatives **3**, a series of control experiments were performed (Scheme 2). We hypothesized that siloxane formation could take place through: (i) the ruthenium catalysed condensation of two silanol

Table 3 Reduction of N_2O with hydrosilanes using Ru·**L4**$^{0.5}$

Entry	Silane	SiH conv. [%]	**2** : **3** ratio
1	Ph_2MeSiH (**1b**)	>99	>99 : 1
2[a]	$(PhCH_2CH_2)Me_2SiH$ (**1c**)	98	>1 : 99
3	$^nPr_3SiH$ (**1d**)	95	58 : 42
4	$^iPr_3SiH$ (**1e**)	0	—
5	$(EtO)_3SiH$ (**1f**)	98	63 : 37

Reaction conditions, unless otherwise noted: 1.0 mol% Ru, 1 bar N_2O, 65 °C, THF. Reaction time: 24 h. Conversion and selectivity were determined by ^{1}H NMR spectroscopy using mesitylene as the internal standard. [a] Reaction time: 48 h.

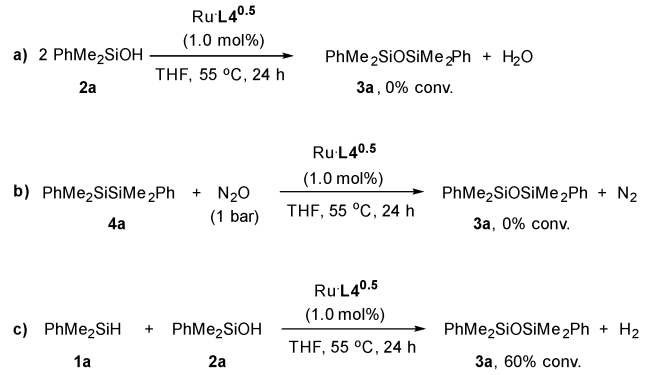

Scheme 2 Control reactions for the formation of the siloxane product **3a**.

molecules (silanol dehydration),[23] (ii) the oxidation of disilane formed through the dehydrogenative coupling of the hydrosilane,[24,25] and/or (iii) the dehydrogenative coupling of silanol and silane.[26] While no reaction was observed when a solution of $PhMe_2SiOH$ (**2a**) in THF was heated to 55 °C in the presence of Ru·**L4**$^{0.5}$ (Scheme 2a) or the disilane $PhMe_2SiSiMe_2Ph$ (**4a**) was made to react with N_2O (Scheme 2b), the reaction of **2a** with silane **1a** under these conditions proceeded with 60% conversion (Scheme 2c). These results are in agreement with the formation of **3a** taking place through a Ru catalysed coupling of silanol and hydrosilane with concomitant H_2 release.

In conclusion, a series of narrowly-dispersed Ru nanoparticles stabilized by tridentate SNS ligands have been prepared and characterized. These materials are able to catalyse the reduction of N_2O, a relevant harmful greenhouse and ozone-depleting gas, with hydrosilanes under relatively mild reaction conditions (1 bar N_2O, 55–65 °C) to yield innocuous N_2 and potentially useful Si–O containing derivatives.

The financial support (FEDER contribution) from the Spanish Agencia Estatal de Investigación (PID2019-104159GB-I00/MCIN/AEI/10.13039/501100011033), Junta de Andalucía (P18-FR-3208 and US-1380604) and CSIC (COOPB20604) is gratefully acknowledged. The ''Talent Attraction Program'' of the University of Cádiz is acknowledged by supporting B. Lacroix contract code E-11-2019-0133241.

Conflicts of interest

There are no conflicts of interest to declare.

Notes and references

1 M. J. Prather, *Science*, 1998, **279**, 1339; A. R. Ravishankara, J. S. Daniel and R. W. Portmann, *Science*, 2009, **326**, 123.
2 J. Hansen and M. Sato, *Proc. Natl. Acad. Sci. U. S. A.*, 2004, **101**, 16109; H. A. Rodhe, *Science*, 1990, **248**, 1217; S. A. Montzka, E. J. Dlugokencky and J. H. Butler, *Nature*, 2011, **476**, 43.
3 E. A. Davidson and D. Kanter, *Environ. Res. Lett.*, 2014, **9**, 105012.
4 M. Jabłońska and R. Palkovits, *Catal. Sci. Technol.*, 2016, **6**, 7671; M. Kjellberg, A. Ohleier, P. Thuéry, E. Nicolas, L. Anthore-Dalion and T. Cantat, *Chem. Sci.*, 2021, **12**, 10266; R. Deeba, F. Molton, S. Chardon-Noblat and C. Costentin, *ACS Catal.*, 2021, **11**, 6099; M. Konsolakis, *ACS Catal.*, 2015, **5**, 639; Ø. Nirisen, D. Waller and D. M. Brackenbury, *Top. Catal.*, 2019, **62**, 1113.
5 For selected examples, see: K. O. Denisova, A. A. Ilyin, R. N. Rumyantsev, A. P. Ilyin and A. V. Volkova, *Russ. J. Gen. Chem.*, 2019, **89**, 1338; K. A. Dubkov, G. I. Panov and V. N. Parmon, *Russ. Chem. Rev.*, 2017, **86**, 510; K. Severin, *Chem. Soc. Rev.*, 2015, **44**, 6375.
6 A. Miyamoto, S. Baba, M. Mori and Y. Murakami, *J. Phys. Chem.*, 1981, **85**, 3117; A. C. Gluhoi, M. A. P. Dekkers and B. E. Nieuwenhuys, *J. Catal.*, 2003, **219**, 197; G. Delahay, M. Mauvezin, A. Guzmán-Vargas and B. Coq, *Catal. Commun.*, 2002, **3**, 385; T. Nobukawa, M. Yoshida, K. Okumura, K. Tomishige and K. Kunimori, *J. Catal.*, 2005, **229**, 374; S. A. Carabineiro and B. E. Nieuwenhuys, *Surf. Sci.*, 2001, **495**, 1; L. Jacobs, C. Barroo, N. Gilis, S. V. Lambeets, E. Genty and T. Visart de Bocarmé, *Appl. Surf. Sci.*, 2018, **435**, 914; X. Huo, D. J. Van Hoomissen, J. Liu, S. Vyas and T. J. Strathmann, *Appl. Catal., B*, 2017, **211**, 188.
7 R. Zeng, M. Feller, Y. Ben-David and D. Milstein, *J. Am. Chem. Soc.*, 2017, **139**, 5720.
8 T. L. Gianetti, S. P. Annen, G. Santiso-Quinones, M. Reiher, M. Driess and H. Grützmacher, *Angew. Chem., Int. Ed.*, 2016, **55**, 1854.
9 X. Chen, H. Wang, S. Du, M. Driess and Z. Mo, *Angew. Chem., Int. Ed.*, 2022, **61**, e202114598.
10 R. A. Pramudita and K. Motokura, *ChemSusChem*, 2021, **14**, 281.
11 P. G. Andersson, I. J. Munslow, ed., *Modern Reduction Methods*, Wiley-VCH; Weinhein, 2008.
12 L. Anthore-Dalion, E. Nicolas and T. Cantat, *ACS Catal.*, 2019, **9**, 11563.
13 S. E. Denmark and C. S. Regens, *Acc. Chem. Res.*, 2008, **41**, 1486; R. Murugavel, A. Voigt, M. G. Walawalkar and H. W. Roesky, *Chem. Rev.*, 1996, **96**, 2205; R. Murugavel, M. G. Walawalkar, M. Dan, H. W. Roesky and C. N. R. Rao, *Acc. Chem. Res.*, 2004, **37**, 763; F. Guida-Pietrasanta and B. Boutevin, *Adv. Polym. Sci.*, 2005, **179**, 1; Y. Abe and T. Gunji, *Prog. Polym. Sci.*, 2004, **29**, 149; H.-H. Moretto, M. Schulze and G. Wagner, *''Silicones''. Ullmann's Encyclopedia of Industrial Chemistry*. Weinheim: Wiley-VCH, 2005; Z. Ren and S. Yan, *Prog. Mater. Sci.*, 2016, **83**, 383.
14 K. Kucinsky, H. Stachowiak-Dłużyńska and G. Hreczycho, *Coord. Chem. Rev.*, 2022, **459**, 214456.
15 K. Philippot and A. Rocoux, *Nanoparticles in Catalysis: Advances in Synthesis and Applications*, Wiley-VCH; Weinheim, 2021.
16 K. Philippot and B. Chaudret, in *Comprehensive Organometallic Chemistry III*, R. H. Crabtree and M. P. Mingos, ed., Elsevier, 2007, Ch. 12–3, Vol. 12.
17 J. M. Asensio, D. Bouzouita, P. W. N. M. van Leeuwen and B. Chaudret, *Chem. Rev.*, 2020, **120**, 1042.
18 J. Schörgenhumer, A. Zimmermann and M. Waser, *Org. Process Res. Dev.*, 2018, **22**, 862.
19 P. Lara, O. Rivada-Wheelaghan, S. Conejero, R. Poteau, K. Phlippot and B. Chaudret, *Angew. Chem., Int. Ed.*, 2011, **50**, 12080.
20 D. J. Morgan, *Surf. Interface Anal.*, 2015, **47**, 1072.
21 L. M. Martínez-Prieto, M. Puche, C. Cerezo-Navarrete and B. Chaudret, *J. Catal.*, 2019, **337**, 429.
22 R. Nyholm and N. Maartensson, *Solid State Phys.*, 1980, **13**, L279; K. W. Park, J.-H. Choi, B.-K. Kwon, S.-A. Lee, Y.-E. Sung, H.-Y. Ha, S.-A. Hong, H. Kim and A. Wieckowski, *J. Phys. Chem. B*, 2002, **106**, 1869; N. Chakroune, G. Viau, S. Ammar, L. Poul, D. Veautier, M. M. Chemini, C. Mangeney, F. Villian and F. Fièvet, *Langmuir*, 2005, **21**, 6788.
23 E. A. Ison, R. A. Corbin and M. M. Abu-Omar, *J. Am. Chem. Soc.*, 2005, **127**, 11938; A. Krüger and M. Albrecht, *Chem. – Eur. J.*, 2012, **18**, 652.
24 M. Okazaki, S. Ohshitanai, H. Tobita and H. Ogino, *Chem. Lett.*, 2001, 952; M. Itazaki, K. Ueda and H. Nakazawa, *Angew. Chem., Int. Ed.*, 2009, **48**, 3313.
25 C. Gryparis and M. Stratakis, *Chem. Commun.*, 2012, **48**, 10751.
26 J. Kaźmierczak, K. Kuciński, D. Lewandowski and G. Hreczycho, *Inorg. Chem.*, 2019, **58**, 1201.